

NEUTRINO PROCESSES IN SUPERNOVAE AND NEUTRON STARS IN THEIR INFANCY AND OLD AGE

M. PRAKASH, S. RATKOVIĆ & S. I. DUTTA

*Department of Physics & Astronomy
State University of New York at Stony Brook
Stony Brook, NY 11794-3800, USA*

PALS*

Neutrino processes in semi-transparent supernova matter, opaque to semi-transparent protoneutron star matter, and catalyzed neutron stars are discussed.

1. Introduction

In recent years, the study of neutrino emission, scattering, and absorption in matter at high density and/or temperature has gained prominence largely due to its importance in a wide range of astrophysical phenomena. Energy loss in degenerate helium cores of red giant stars,^{1,2} cooling in pre-white dwarf interiors,³ the short- and long-term cooling of neutron stars,^{4,5} the deflagration stages of white dwarfs which may lead to type Ia supernovae,^{6,7} explosive stages of type II (core-collapse) supernovae,⁸ and thermal emission in accretion disks of gamma-ray bursters,^{9,10} are examples in which neutral and charged current weak interaction processes that involve neutrinos play a significant role. Since this is a vast subject, we will highlight some recent developments in the context of core-collapse supernovae and neutron stars from their birth to old age.

2. Supernovae

In unravelling the mechanism by which a type-II supernova explodes, the implementation of accurate neutrino transport has been realized to be critical.¹¹ The basic microphysical inputs of accurate neutrino transport

*Friends who have helped and contributed significantly; see the Acknowledgements.

coupled in hydrodynamical situations are the differential neutrino production and absorption rates and their associated emissivities. The processes and precise forms in which such inputs are required for multienergy treatment of neutrinos for both sub-nuclear and super-nuclear densities (nuclear density $\rho_0 \simeq 2.65 \times 10^{14} \text{ g cm}^{-3}$) are detailed in Refs. [12, 13].

At sub-nuclear densities, the relevant processes are:

$$\text{pair production : } e^+ + e^- \rightarrow \nu + \bar{\nu}, \quad (1)$$

$$\text{the photo - neutrino process : } e^\pm + \gamma^* \rightarrow e^\pm + \nu + \bar{\nu}, \quad (2)$$

$$\text{the plasma process : } \gamma^* \rightarrow \nu + \bar{\nu}, \quad (3)$$

$$\text{nucleon - nucleon bremsstrahlung : } (n, p) \rightarrow (n, p) + \nu + \bar{\nu}, \text{ and } (4)$$

$$\nu - \text{flavor production : } \nu_i + \bar{\nu}_i \rightarrow \nu_j + \bar{\nu}_j. \quad (5)$$

The relative importance of these processes depends on the temperature and density of ambient matter and is sketched in Figure 1.

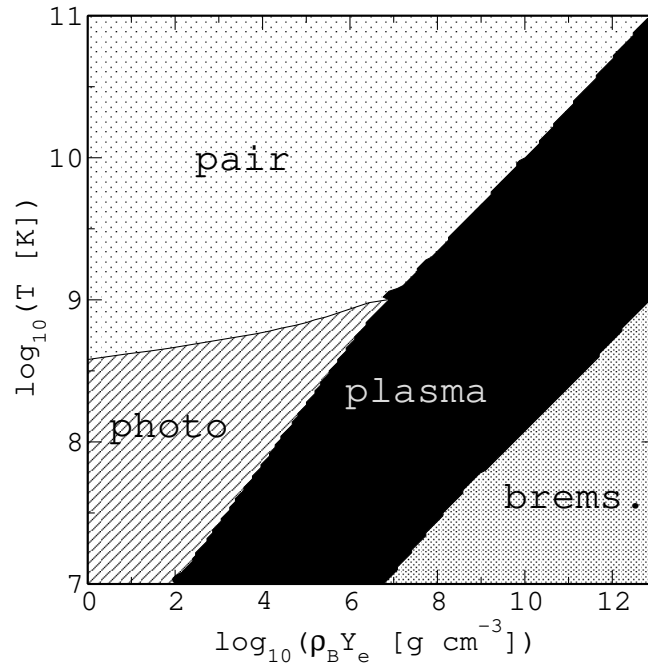


Figure 1. Regions of temperature and density in which the various neutrino emitting processes are operative.

Additional neutrino processes in the supernova environment include

$$p + e^- \rightarrow n + \nu_e, \quad (A, Z) + e^- \rightarrow (A, Z - 1) + \nu_e, \quad (6)$$

$$\nu + (A, Z) \rightarrow \nu + (A, Z), \quad (7)$$

$$\nu + e^- \rightarrow \nu + e^-, \quad \nu + (A, Z) \rightarrow \nu + (A, Z)^*, \quad (8)$$

$$(A, Z)^* \rightarrow (A, Z) + \nu + \bar{\nu}. \quad (9)$$

Reactions (6) begin the process of neutronization and decrease of lepton number per baryon Y_L , whose value after ν -trapping determines the masses of the homologous core and initial PNS, and thus the available energy for the shock and subsequent neutrino emissions. The equation of state also influences these quantities, most importantly through the nuclear symmetry energy. In the subnuclear density regime, the coherent scattering reaction (7) from nuclei in a lattice is the most important opacity source. The reactions (8) are important in changing the neutrino energy and in achieving thermodynamic equilibrium. The reactions (1) and (9) are also important in achieving thermodynamic equilibrium. The bremsstrahlung and modified Urca ($n + p \rightarrow n + n + e^+ + \nu + \bar{\nu}$) processes dominate in many circumstances. For example, the production and thermalization of μ and τ neutrinos, which receives contributions from reactions (1) through (5), and (9), is dominated by nucleon bremsstrahlung (4) for number density $n > 0.005 \text{ fm}^{-3}$ and temperature $T < 15 \text{ MeV}$. The modified Urca process dominates the cooling of protoneutron stars if direct Urca processes involving nucleons, hyperons or other strange particles do not occur.

3. Kernels for Neutrino Transport Calculations

The evolution of the neutrino distribution function f , generally described by the Boltzmann transport equation in conjunction with hydrodynamical equations of motion together with baryon and lepton number conservation equations, is

$$\frac{\partial f}{\partial t} + v^i \frac{\partial f}{\partial x^i} + \frac{\partial(fF^i)}{\partial p^i} = B_{EA}(f) + B_{NES}(f) + B_{\nu N}(f) + B_{TP}(f). \quad (10)$$

Here, F^i is the force acting on the particle and we have ignored general relativistic effects for simplicity (see, for example, Ref. [12] for full details). The right hand side of the above equation is the neutrino source term in which, $B_{EA}(f)$ incorporates neutrino emission and absorption processes,

$B_{NES}(f)$ accounts for the neutrino-electron scattering process, $B_{\nu N}(f)$ includes scattering of neutrinos off nucleons and nuclei, and $B_{TP}(f)$ considers the thermal production and absorption of neutrino-antineutrino pairs.

Till recently, detailed differential information was not available for the plasma and photoneutrino processes. In prior works in which the total rates and emissivities for these processes were computed, the energy and angular dependences of the emitted neutrinos with 4-momenta q and q' were eliminated by using Lenard's identity:

$$\int \frac{d^3q}{2E_q} \frac{d^3q'}{2E_{q'}} \delta^4(q_t - q - q') q^\mu q'^\nu = \frac{\pi}{24} \Theta(q_t^2) (2q_t^\mu q_t^\nu + q_t^2 g^{\mu\nu}). \quad (11)$$

Although the use of this identity simplifies considerably the calculation of the total emissivity, differential information about the neutrinos is entirely lost. On the other hand, calculations of differential rates and emissivities, such as

$$\frac{d^3\Gamma}{dE_q dE_{q'} d(\cos\theta_{qq'})} \quad \text{and} \quad \frac{d^3Q}{dE_q dE_{q'} d(\cos\theta_{qq'})}, \quad (12)$$

where $\theta_{qq'}$ is the angle between the neutrino pairs, entail the calculation of the relevant squared matrix elements hitherto bypassed in obtaining the total rates and emissivities. Realizing this, the squared matrix elements for the plasma and photoneutrino processes were computed in Refs. [16, 17]. Some results from these recent works are highlighted below.

3.1. The Plasma Process

As is well known, e^+e^- pairs in a plasma cause the photon to acquire an effective mass, which arises from electromagnetic interactions (cf. Refs. [16, 18] and references therein). Therefore, we can consider the photon to be a massive spin-1 particle that couples to the $\nu\bar{\nu}$ pair through the two one-loop diagrams shown in Figure 2.

Suppressing the dependencies on (r, t) for notational simplicity, the source term for the plasma process can be written as

$$B(f) = [1 - f] \frac{1}{(2\pi)^3} \int_0^\infty E_2^2 dE_2 \int_{-1}^1 d\mu_2 \int_0^{2\pi} d\phi_2 R^P(E_1, E_2, \cos\theta) [1 - \bar{f}] \\ - f \frac{1}{(2\pi)^3} \int_0^\infty E_2^2 dE_2 \int_{-1}^1 d\mu_2 \int_0^{2\pi} d\phi_2 R^A(E_1, E_2, \cos\theta) \bar{f}, \quad (13)$$

where the first and the second terms correspond to the source (neutrino gain) and sink (neutrino loss) terms, respectively. E_1 and E_2 are the energies of the neutrino and antineutrino, respectively. Angular variables

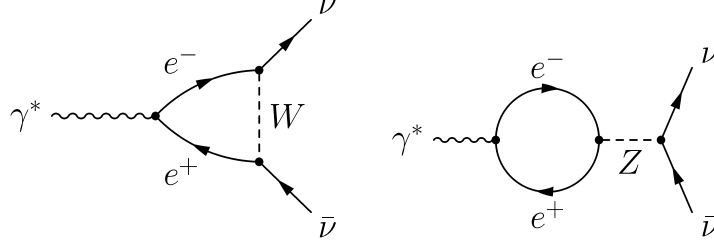


Figure 2. Leading order Feynman diagrams describing the emission of a neutrino pair from the plasma process. The charged current process in which the W -boson is exchanged produces only $\nu_e \bar{\nu}_e$, while that in which the neutral Z -boson is exchanged results in pairs of all three neutrino (e , μ , and τ) flavors.

$\mu_i \equiv \cos \theta_i$ and ϕ_i ($i = 1, 2$) are defined with respect to the z -axis that is locally set parallel to the outgoing radial vector \mathbf{r} . The angle θ between the neutrino and antineutrino pair is related to θ_1 and θ_2 through

$$\cos \theta = \mu_1 \mu_2 + \sqrt{(1 - \mu_1^2)(1 - \mu_2^2)} \cos(\phi_1 - \phi_2). \quad (14)$$

Notice that $f \equiv f(E_1, \mu_1)$ and $\bar{f} \equiv \bar{f}(E_2, \mu_2)$. The production and absorption kernels are given by

$$R_a^p(E_1, E_2, \cos \theta) = \int \frac{d^3 k}{(2\pi)^3} Z_Y(k) \left(\frac{\xi n_B(\omega, T)}{1 + n_B(\omega, T)} \right) \times \frac{1}{8\omega E_1 E_2} \delta^4(K - Q_1 - Q_2) (2\pi)^4 \langle |\mathcal{M}|^2 \rangle, \quad (15)$$

where the subscript Y stands for T -“transverse” or L -“longitudinal”. The factor ξ accounts for the spin averaging; $\xi = 2$ for the transverse, axial and mixed cases, while for the longitudinal case $\xi = 1$.

The angular dependences in the kernels $R_a^p(E_1, E_2, \cos \theta)$ are often expressed in terms of Legendre polynomials as

$$R_a^p(E_1, E_2, \cos \theta) = \sum_{l=0}^{\infty} \frac{2l+1}{2} \Phi_l^p(E_1, E_2) P_l(\cos \theta), \quad (16)$$

where the Legendre coefficients $\Phi_l^p(E_1, E_2)$ depend exclusively on energies.

From Eq. (15), it is evident that the kernels are related to the neutrino rates and emissivities. We first consider the production kernel $R^p(E_1, E_2, \cos \theta)$. The corresponding analysis for the absorption kernel $R^a(E_1, E_2, \cos \theta)$ can be made along the same lines, but with the difference

that n_B is replaced by $1 + n_B$. The neutrino production rate is given by

$$\begin{aligned}\Gamma &= \xi \int \frac{d^3k}{(2\pi)^3 2\omega} Z_Y(k) \frac{d^3q_1}{(2\pi)^3 2E_1} \frac{d^3q_2}{(2\pi)^3 2E_2} \\ &\quad \times n_B(\omega, T) \delta^4(K - Q_1 - Q_2) (2\pi)^4 \langle |\mathcal{M}|^2 \rangle \\ &= \int \frac{d^3q_1}{(2\pi)^3} \frac{d^3q_2}{(2\pi)^3} R^p(E_1, E_2, \cos\theta),\end{aligned}\quad (17)$$

which defines the kernel $R^p(E_1, E_2, \cos\theta)$ and is to be identified with that in Eq. (15). The emissivity Q can also be cast in terms of R^p using

$$Q = \int \frac{d^3q_1}{(2\pi)^3} \frac{d^3q_2}{(2\pi)^3} (E_1 + E_2) R^p(E_1, E_2, \cos\theta). \quad (18)$$

The Legendre coefficients Φ_l^p for the transverse part of the production kernels are shown in Figure 3 for $l = 0$ through 3. The longitudinal component becomes comparable to the transverse component only in the strongly degenerate regime (see Figure 4), while the axial and mixed components (the latter contributes only to the differential rates and emissivities but not to the total, since it is anti-symmetric in E_1 and E_2) are negligibly small. Notice that the first few Legendre coefficients are all comparable in magnitude. Moreover, the emission process is anisotropic (see also Figure 7 of Ref. 16). “Light” photon ($\omega_p \ll T$) decays result in neutrino pairs with small outgoing angles between them, whereas “massive” photons ($\omega_p \gg T$) yield back-to-back neutrino emission.

Figure 4 shows the individual contributions to the total emissivity from the transverse, longitudinal, and axial channels at $T = 10^{11}\text{K}$ and $T = 10^9\text{K}$, respectively. The curves show results from expressions derived by exploiting the Lenard identity.^{16,18} The symbols “ \times ” and “+” show results obtained by integrations of the differential emissivities. At all densities and temperatures, the contribution of the axial channel to the total emissivity is negligible. For each temperature, the emissivity in the transverse channel dominates over that of the longitudinal channel at low densities. However, the peak values in these two channels are attained at nearly the same density; thereafter their individual contributions coincide.

In terms of the density and temperature dependencies of the plasma frequency ω_p and the electron chemical potential μ_e (see Figure 4 of Ref. [16]), a detailed qualitative and quantitative analyses of the basic features of Figure 4 are provided in Ref. [16]. Consider the case of Q_T first. At a fixed temperature, the basic features to note are:

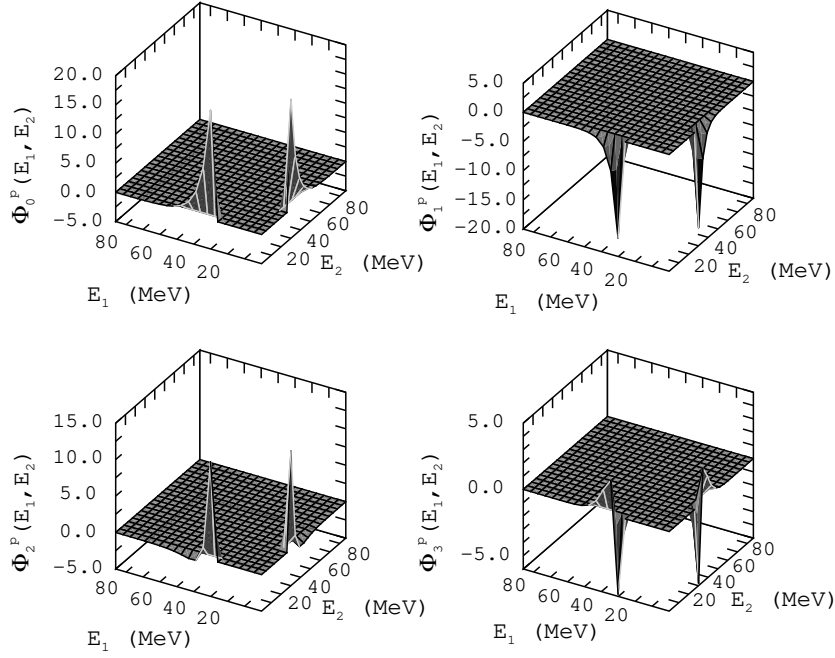


Figure 3. The transverse part of the production kernels for $T = 8.62$ MeV and $\rho_B Y_e < 10^{10}$ g cm $^{-3}$. The Legendre coefficients Φ_l^P are shown for $l = 0$ through 3. The neutrino energies E_1 and E_2 are in MeV and the Legendre coefficients are in units of 10^{129} \hbar^6 erg $^{-6}$ cm 3 s $^{-7}$.

- (1) Q_T is independent of the density $\rho_B Y_e$ until a turn-on density $(\rho_B Y_e)_{to}$ is reached,
- (2) For densities larger than this turn-on density, Q_T exhibits a power-law rise until a maximum is reached at $(\rho_B Y_e)_{peak}$, and
- (3) For $\rho_B Y_e \gg (\rho_B Y_e)_{peak}$, the fall-off with density is exponential.

In the case of $T \gg \omega_p$ (non-degenerate plasma), the main contribution

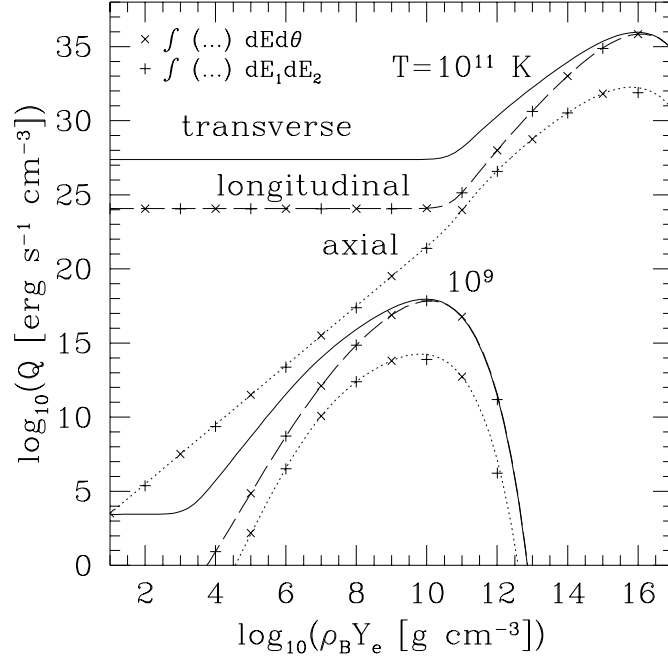


Figure 4. Individual contributions from the transverse, longitudinal, and axial channels to the neutrino emissivity. The mass density of protons in the plasma, $\rho_B Y_e = m_p n_e$, where m_p is the proton mass, $Y_e = n_e/n_B$ is the net electron fraction (n_B is the baryon number density), and n_e is net electron number density.

to Q_T comes from high photon momenta. To a very good approximation,¹⁸

$$Q_T \simeq \frac{2 \sum_f (C_V^f)^2 G_F^2}{48\pi^4 \alpha} \zeta(3) m_T^6 T^3, \quad (19)$$

where $\zeta(3) \simeq 1.202$ is Riemann's Zeta function and m_T is the transverse photon mass.

For $T \ll \omega_p$ (degenerate plasma), Q_T takes the form¹⁸

$$Q_T \simeq \frac{\sum_f (C_V^f)^2 G_F^2}{48\pi^4 \alpha} \sqrt{\frac{\pi}{2}} \omega_p^{15/2} T^{3/2} e^{-\omega_p/T}. \quad (20)$$

The analyses of the longitudinal and axial emissivities can be carried out along the same lines as that for the transverse emissivity.¹⁶

3.2. The Photoneutrino Process

The leading order diagrams for the photoproduction of neutrino pairs, $e^\pm + \gamma^* \rightarrow e^\pm + \nu_{e,\mu,\tau} + \bar{\nu}_{e,\mu,\tau}$, are shown in Figure 5. The kernels of the collision integral for the photoneutrino process can be calculated along the same lines as for the plasma process and are detailed in Ref. 17.

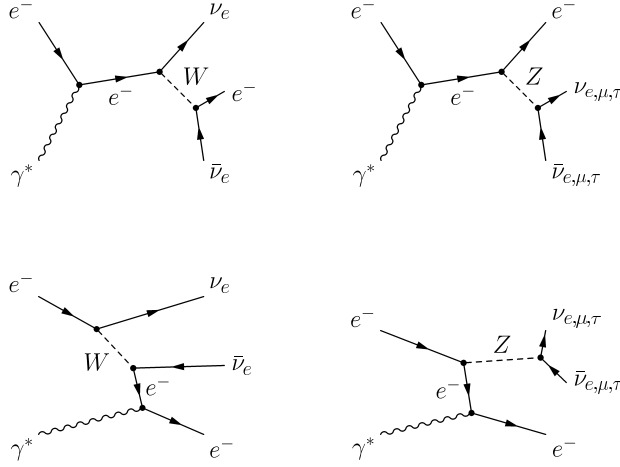


Figure 5. Leading order Feynman diagrams describing the emission of a neutrino pair from the photoneutrino process. The charged current W - exchange channel produces only $\nu_e \bar{\nu}_e$, whereas the neutral Z - exchange results in pairs of all three neutrino (e , μ , and τ) flavors. Contributions from positrons are obtained by the replacement $e^- \rightarrow e^+$.

Numerical results for the symmetric and anti-symmetric components of $\Phi_0^p(E_q, E_{q'})$ and $\Phi_1^p(E_q, E_{q'})$ are shown in Figure 6 for the case $T = 10^{11}$ K = 8.62 MeV and $\rho_B Y_e = 1 \text{ g cm}^{-3}$. The results explicitly show the expected symmetry properties in neutrino energies E_q and $E_{q'}$. A comparison of the relative magnitudes $\Phi_1^p(E_q, E_{q'})$ (not shown here, but see Figure 6 of Ref. [17]) and $\Phi_0^{p(\text{sym})}(E_q, E_{q'})$ shows that the $l = 0$ term is the dominant term. The magnitude of $\Phi_0^{p(\text{asym})}$ amounts to only 10% of the leading $\Phi_0^{p(\text{sym})}$ contribution. The contributions of $\Phi_1^{p(\text{sym})}$ and $\Phi_1^{p(\text{asym})}$ are 6% and 3%, respectively. In physical terms, this means that neutrino-pair emission from the photo-neutrino process is dominantly isotropic. Therefore, depending on the required accuracy, $\Phi_0^{p(\text{sym})}$ might be adequate in practical applications. Note also that that the production kernels are negligible for energies E_q and $E_{q'} \gtrsim 10T$.

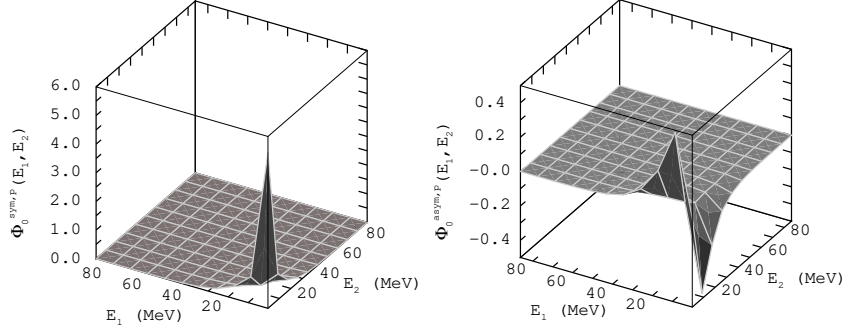


Figure 6. Symmetric and anti-symmetric parts of the Legendre coefficients $\Phi_0^{p(\text{sym})}$ and $\Phi_0^{p(\text{asym})}$ in the production kernels for the transverse case. The ν -energies E_q and $E_{q'}$ are in MeV and the Legendre coefficients are in units of $10^{129} \hbar^6 \text{ erg}^{-6} \text{ cm}^3 \text{ s}^{-7}$.

Contributions of the transverse and longitudinal components to the total emissivity are shown in Figure 7. For all temperatures at sufficiently high net electron densities n_e (i.e., a degenerate plasma), the inequalities

$$\begin{aligned} \mu_e &\gg T, \quad \mu_e \gg m_e, \\ \omega_P &\gg T, \quad \omega_P \gg m_e \end{aligned} \quad (21)$$

are satisfied. In this case,

$$Q_T \simeq \frac{4}{3} \frac{\alpha G_F^2 (C_V^2 + C_A^2)}{(2\pi)^6} \omega_p^6 T^3 e^{-\omega_p/T}. \quad (22)$$

The nondegenerate situation occurs at sufficiently low densities for which $\mu_e - m_e \ll T$. In this case, both Q_T and Q_L exhibit a plateau for temperatures $T \geq 10^9$ K. The emissivity and rate can be expressed in terms of the simple expressions

$$\left(\frac{Q_T}{\Gamma_T} \right) = \frac{20\alpha G_F^2 (C_V^2 + C_A^2)}{3(2\pi)^6} \left(\frac{T^9 \times 775.54}{T^8 \times 136.50} \right). \quad (23)$$

The significance of the detailed differential rates and emissivities of neutrino emission and absorption processes in calculations of core-collapse supernovae in which neutrino transport is strongly coupled with hydrodynamics remains to be explored.

4. Protoneutron Stars

A protoneutron star (PNS) is born in the aftermath of the gravitational collapse of the core of a massive star accompanying a successful super-

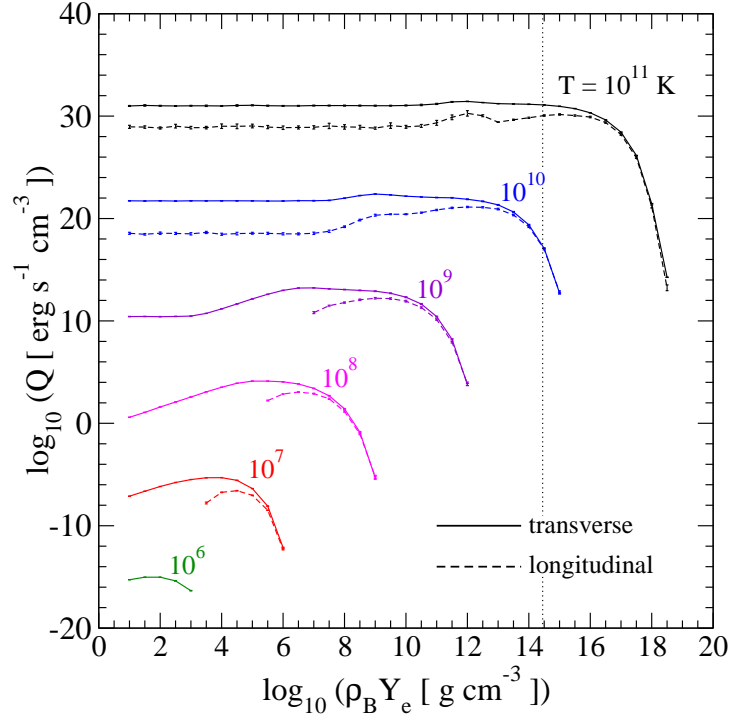


Figure 7. Individual contributions from the transverse and longitudinal channels to the neutrino emissivity as a function of baryon density at the indicated temperatures. The error bars show the variance of the Monte Carlo integration. For densities in excess of nuclear density shown by the dotted vertical line, neutrino production from strongly interacting particles dominate over QED-plasma processes.

nova explosion. During the first tens of seconds of evolution, nearly all ($\sim 99\%$) of the remnant's binding energy is radiated away in neutrinos of all flavors.^{19,22,23,24,25,26} The neutrino luminosities and the emission timescale are controlled by several factors, such as the total mass of the PNS and the opacity at supranuclear density, which depends on the composition and dense matter equation of state (EOS). One of the chief objectives in modeling PNS's is to infer their internal compositions from neutrino signals detected from future supernovae by SuperK, SNO and others under consideration, including UNO.²⁷

4.1. The Evolution of a Protoneutron Star

The evolution of a PNS proceeds through several distinct stages^{19,20} and with various outcomes,²¹ as shown schematically in Figure 8. Immediately following core bounce and the passage of a shock through the outer PNS's mantle, the star contains an unshocked, low entropy core of mass $\simeq 0.7 M_{\odot}$ in which neutrinos are trapped (stage 1 in the figure). The core is surrounded by a low density, high entropy ($5 < s < 10$) mantle that is both accreting matter from the outer iron core falling through the shock and also rapidly losing energy due to electron captures and thermal neutrino emission. The mantle extends up to the shock, which is temporarily stalled about 200 km from the center prior to an eventual explosion.

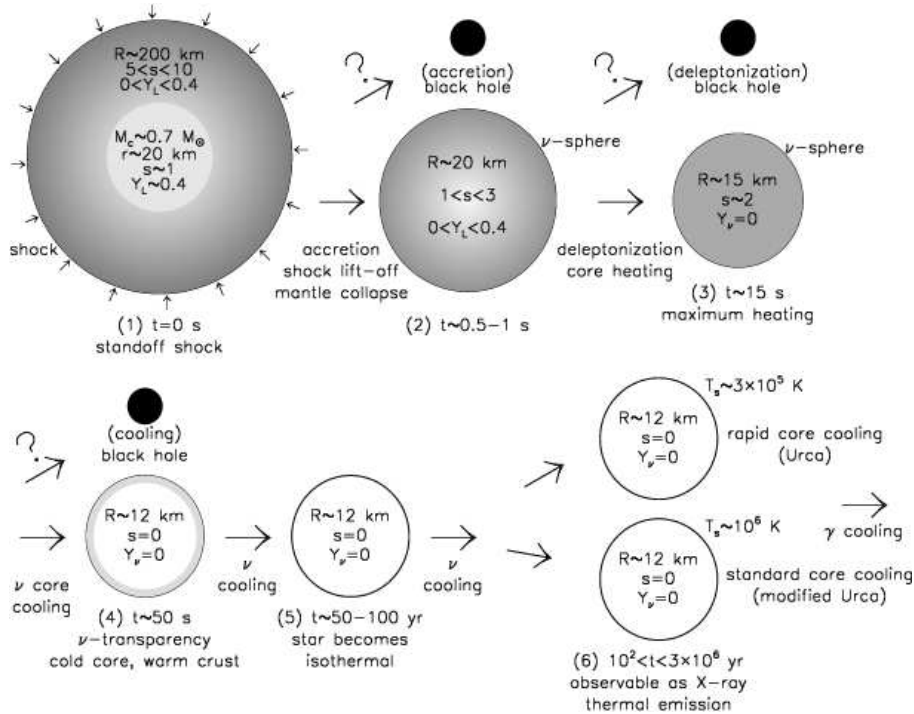


Figure 8. The main stages of evolution of a protoneutron star. Shading approximately indicates relative temperatures.

After a few seconds (stage 2), accretion becomes less important if the supernova is successful and the shock has ejected the stellar envelope. Ex-

tensive neutrino losses and deleptonization will have led to a loss of lepton pressure and the collapse of the mantle. If enough accretion has occurred, however, the star's mass could increase beyond the maximum mass capable of being supported by the hot, lepton-rich matter. If this occurs, the remnant collapses to form a black hole and its neutrino emission is believed to quickly cease.²⁸

Neutrino diffusion deleptonizes the core on time scales of 10–15 s (stage 3). Diffusion time scales are proportional to $R^2(c\lambda_\nu)^{-1}$, where R is the star's radius and λ_ν is the effective neutrino mean free path. This generic relation illustrates how both the EOS and the composition influence evolutionary time scales. The diffusion of high-energy (200–300 MeV) ν 's from the core to the surface where they escape as low-energy (10–20 MeV) ν 's generates heat (a process akin to joule heating). The core's entropy approximately doubles, producing temperatures in the range of 30–60 MeV during this time, even as neutrinos continue to be prodigiously emitted from the star's effective surface, or ν -sphere.

Strange matter, in the form of hyperons, a Bose condensate, or quark matter, suppressed when neutrinos are trapped, could appear at the end of the deleptonization. Its appearance would lead to a decrease in the maximum mass that matter is capable of supporting, implying metastability of the neutron star and another chance for black hole formation.²¹ This would occur if the PNS's mass, which must be less than the maximum mass of hot, lepton-rich matter (or else a black hole would already have formed), is greater than the maximum mass of hot, lepton-poor matter. However, if strangeness does not appear, the maximum mass instead increases during deleptonization and the appearance of a black hole would be unlikely unless accretion in this stage remains significant.

The PNS is now lepton-poor, but it is still hot. While the star has zero net neutrino number, thermally produced neutrino pairs of all flavors dominate the emission. The average neutrino energy slowly decreases, and the neutrino mean free path increases. After approximately 50 seconds (stage 4), $\lambda \simeq R$, and the star finally becomes transparent to neutrinos. Since the threshold density for the appearance of strange matter decreases with decreasing temperature, a delayed collapse to a black hole is still possible during this epoch.

Following the onset of neutrino transparency, the core continues to cool by neutrino emission, but the star's crust remains warm and cools less quickly. The crust is an insulating blanket which prevents the star from coming to complete thermal equilibrium and keeps the surface relatively

warm ($T \approx 3 \times 10^6$ K) for up to 100 years (stage 5). The temperature of the surface after the interior of the star becomes isothermal (stage 6) is determined by the rate of neutrino emission in the star's core and the composition of the surface.

4.2. Neutrino Signals in Terrestrial Detectors

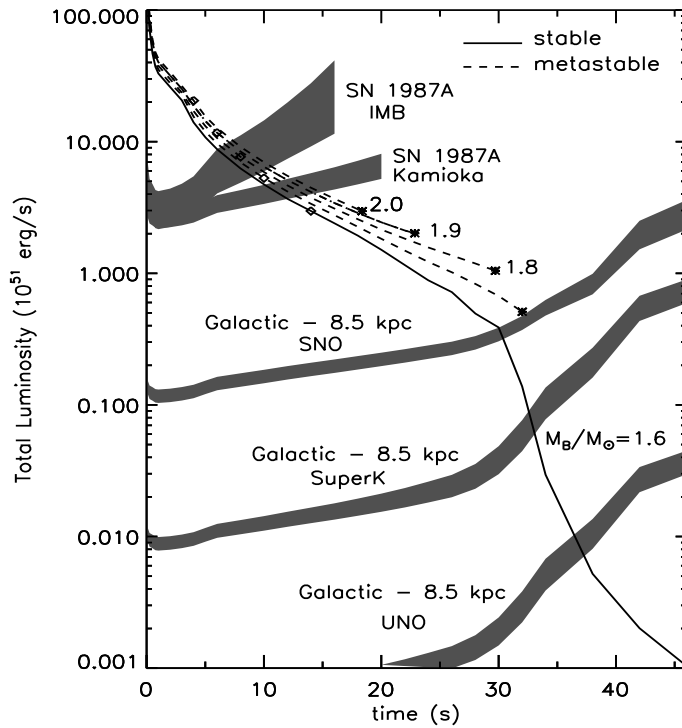


Figure 9. The evolution of the total neutrino luminosity for npQ PNS's. Shaded bands illustrate the limiting luminosities corresponding to a count rate of 0.2 Hz, assuming a supernova distance of 50 kpc for IMB and Kamioka, and 8.5 kpc for SNO and SuperK. The widths of the shaded regions represent uncertainties in the average neutrino energy from the use of a diffusion scheme for neutrino transport.

A comparison of the signals observable with different detectors is shown in Figure 9, which displays L_ν as a function of baryon mass M_B for stars containing quarks in their cores. In the absence of accretion, M_B remains

constant during the evolution, while the gravitational mass M_G decreases. The two upper shaded bands correspond to estimated SN 1987A (50 kpc distance) detection limits with KII and IMB, and the lower bands correspond to estimated detection limits in SNO, SuperK, and UNO, for a Galactic supernova (8.5 kpc distance). The detection limits have been set to a count rate $dN/dt = 0.2$ Hz.²⁵ It is possible that this limit is too conservative and could be lowered with identifiable backgrounds and knowledge of the direction of the signal. The width of the bands represents the uncertainty in $\langle E_{\bar{\nu}_e} \rangle$ due to the diffusion approximation.^{24,25,26} It is possible to distinguish between stable and metastable stars, since the luminosities when metastability is reached are always above conservative detection limits.

4.3. *Metastable Protoneutron Stars*

Protoneutron stars in which strangeness appears following deleptonization can be metastable if their masses are large enough. One interesting diagnostic that could shed light on the internal composition of neutron stars would be the abrupt cessation of the neutrino signal. This would be in contrast to a normal star of similar mass for which the signal continues to fall until it is obscured by the background. In Figure 10 the lifetimes for stars containing hyperons (npH), kaons (npK) and quarks (npQ) are compared.²⁵ In all cases, the larger the mass, the shorter the lifetime. For the kaon and quark PNSs, however, the collapse is delayed until the final stage of the Kelvin-Helmholtz epoch, while this is not necessarily the case for hyperon-rich stars. In addition, there is a much stronger mass dependence of the lifetimes for the hyperon case.

Clearly, the observation of a single case of metastability, and the determination of the metastability time alone, will not necessarily permit one to distinguish among the various possibilities. Only if the metastability time is less than 10–15 s, could one decide on this basis that the star's composition was that of npH matter. However, as in the case of SN 1987A, independent estimates of M_B might be available.²⁹ In addition, the observation of two or more metastable neutron stars might permit one to differentiate among these models.

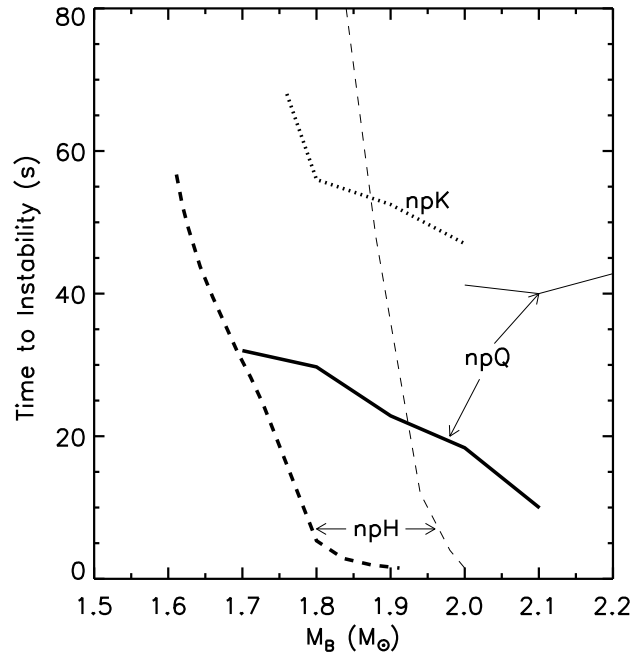


Figure 10. Lifetimes of metastable stars versus the PNS baryon mass M_B . Thick lines denote cases in which the maximum gravitational masses of cold, catalyzed stars are near $1.45 M_\odot$, which minimizes the metastability lifetimes. The thin lines for the npQ and npH cases are for EOSs with larger maximum gravitational masses (1.85 and $1.55 M_\odot$, respectively.)

5. Neutron Stars in Their Old Age

See the contribution from Dany Page to this symposium.

6. Outlook

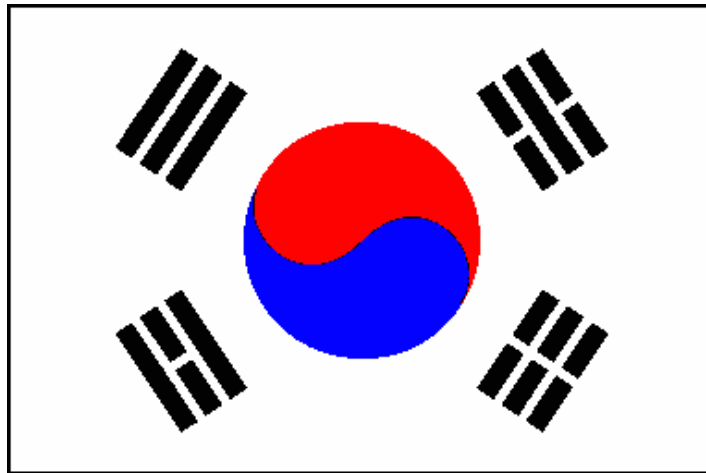
The advent of new-generation neutrino detectors such as Super-Kamiokande and the Sudbury Neutrino Observatory promises thousands of neutrino events in the next Galactic supernova. These will provide crucial diagnostics for the supernova mechanism, important limits on the released binding energy and the remnant mass, and critical clues concerning the composition of high density matter. Research in this area will ascertain the extent to which neutrino transport is instrumental in making a supernova explode. Other bonuses include the elucidation of the possible role of

supernovae and neutrinos in r -process nucleosynthesis.

The main issues that emerge from PNS studies concern the metastability and subsequent collapse to a black hole of a PNS containing quark matter, or other types of matter including hyperons or a Bose condensate, which could be observable in the ν signal. However, discriminating among various compositions may require more than one such observation. This highlights the need for breakthroughs in lattice simulations of QCD at finite baryon density in order to unambiguously determine the EOS of high density matter. In the meantime, intriguing possible extensions of supernova and PNS simulations with npQ and npK matter include the consideration of heterogeneous structures and quark matter superfluidity.³⁰ See also the contribution from Sanjay Reddy to this symposium.

7. Conclusions

감사합니다



Acknowledgements

MP thanks his “PALS” Paul Ellis, Jim Lattimer, Jose Miralles, Dany Page, Jose Pons, Sanjay Reddy, and Andrew Steiner for beneficial collaborations. Research support from DOE grants FG02-88ER-40388 and FG02-87ER-40317 (for MP, SR and SID), and NSF Grant No. 0070998 (for SID), and travel support under the cooperative agreement DE-FC02-01ER41185 for the SciDaC project “Shedding New Light on Exploding Stars: Terascale Simulations of Neutrino-Driven Supernovae and Their Nucleosynthesis” (for MP, SR and SID) are gratefully acknowledged.

References

1. A. V. Sweigart and P. G. Gross, *Astrophys. J. Suppl. Ser.* **36**, 405 (1978).
2. G. G. Raffelt, *Phys. Rep.* **333**, 593 (2000).
3. M. S. O’Brien and S. D. Kawaler, *Astrophys. J.* **539**, 372 (2000).
4. M. Prakash, J. M. Lattimer, R. F. Sawyer, and R. R. Volkas, *Ann. Rev. Nucl. Part. Sci.* **51**, 295 (2001).
5. D. G. Yakovlev, A. D. Kaminker, O. Y. Gnedin, and P. Haensel, *Phys. Rep.* **354**, 1 (2001).
6. W. Hillebrandt and J. C. Niemeyer, *Ann. Rev. Astron. and Astrophys.* **38**, 191 (2000).
7. K. Iwamoto, *et al.*, *Astrophys. J. Suppl. Ser.* **125**, 439 (1999).
8. A. Burrows, *Nature*, **403**, 727 (2000).
9. T. Di Matteo, R. Perna, and R. Narayan, *Astrophys. J.* **579**, 706 (2002).
10. K. Kohri and S. Mineshige, *Astrophys. J.* **577**, 311 (2002).
11. O. E. B. Messer, A. Mezzacappa, S. W. Bruenn, and M. W. Guidry, *Astrophys. J.* **507**, 353 (1998); S. Yamada, H-Th Janka, H. Suzuki, *Astron. Astrophys.* **344**, 533 (1999); A. Burrows, T. Young, P. Pinto, R. Eastman, T. A. Thompson, *Astrophys. J.* **539**, 865 (2000); M. Rampp, H-Th Janka, *Astrophys. J.* **539**, L33 (2000); M. Liebendoerfer, *et al. Phys. Rev.* **D63**, 104003 (2001).
12. S. W. Bruenn, *Astrophys. J. Suppl. Ser.* **58**, 771 (1985).
13. A. Burrows and T. A. Thompson, *astro-ph/0211404*.
14. S. Hammett and G. Raffelt, *Astrophys. J.* **507**, 339 (1998).
15. R. Buras, H-T. Janka, M. Th. Keil, G. G. Raffelt, and M. Rampp, *Astrophys. J.* **587**, 320 (2003).
16. S. Ratkovic, S. I. Dutta and M. Prakash *Phys. Rev.* **D67**, 123002 (2003).
17. S. I. Dutta, S. Ratkovic and M. Prakash *Phys. Rev.* **D69**, 023005 (2004).
18. E. Braaten and D. Segel, *Phys. Rev.* **D48**, 1478-1491 (1993).
19. A. Burrows and J. M. Lattimer, *Astrophys. J.* **307**, 178 (1986).
20. A. Burrows A, *Ann. Rev. Nucl. Sci.* **40**, 181 (1990).
21. M. Prakash, I. Bombaci, Manju Prakash, P. J. Ellis, J. M. Lattimer, and R. Knorren, *Phys. Rep.* **280**, 1 (1997); P. J. Ellis, J. M. Lattimer and M. Prakash, *Comm. Nucl. Part. Phys.* **22**, 63 (1996); M. Prakash, J. R. Cooke,

- J. M. Lattimer, *Phys. Rev.* **D52**, 661 (1995); A. W. Steiner, M. Prakash, J. M. Lattimer, *Phys. Lett.* **B486**, 239 (2000).
22. W. Keil and H-T Janka, *Astron. & Astrophys.* **29**, 145 (1995).
23. A. Burrows and R. F. Sawyer, *Phys. Rev.* **C59**, 510 (1999).
24. J. A. Pons, S. Reddy, M. Prakash, J. M. Lattimer, J. A. Miralles, *Astrophys. J.* **513**, 780 (1999).
25. J. A. Pons, J. A. Miralles, M. Prakash, J. M. Lattimer, 2001. *Astrophys. J.*, **553**, 382 (2001).
26. J. A. Pons, A. W. Steiner, M. Prakash, J. M. Lattimer, 2001. *Phys. Rev. Lett.* **86**, 5223 (2001).
27. C. K. Jung, In *Next Generation Nucleon Decay and Neutrino Dectector*, ed. by Diwan N, Jung CK (AIP, New York, 2000), 29.
28. A. Burrows, *Astrophys. J.* **334**, 891 (1988).
29. F. K. Thielemann, M. Hashimoto and K. Nomoto, 1990. *Astrophys. J.* **349**, 222 (1990); H. A. Bethe and G. E. Brown, *Astrophys. J. Lett.* **445**, L129 (1995).
30. G. W. Carter and S. Reddy, *Phys. Rev.* **D62**, 103002 (2000); S. Reddy, M. Sadziokowski, and M. Tachibana, *Nucl. Phys.* **A714**, 337 (2003); *Phys. Rev. D* **68**, 053010 (2003).